ARCHIVES
of
FOUNDRY ENGINEERING
10.24425/afe.2026.157986
Published quarterly as the organ of the Foundry Commission of the Polish Academy of Sciences
ISSN (2299-2944)
Volume 2026
Issue 2/2026
21 – 32
3/2

Simulation and Verification of Liner ($ZGMn_{13}Cr_2$) Investment Casting Based on Modified Porous Media Equivalent Thermal Conductivity Model

Jingwei Ran [a], Dinghao Guo [a], Zhengwei Yang [b], Bo Lin [b], Zhengtao Ma [b], Xishan Wang [a], Zhiping Xie [a], Rong Li [a] *
[a] School of Mechanical & Electrical Engineering, Guizhou Normal University, China
[b] Guizhou Lines Machine Design and Manufacture Co., LTD, China
* Corresponding author: E-mail address: lirong9242001@163.com

Received 20.11.2025; accepted in revised form 02.04.2026; available online 24.06.2026

Abstract

For the investment casting of $ZGMn_{13}Cr_2$ high-manganese steel porous liners, internal cavities can cause distortion in traditional numerical simulation of the temperature field and defect prediction. In this study, the Bruggeman porous medium equivalent thermal conductivity model was introduced and modified to suit porous castings. After calculating the overall porosity of the liner casting, an equivalent thermal conductivity scaling factor of 0.675 for the liner was derived based on the modified Bruggeman model, and simulations of the liner were carried out in ProCAST software using this correction factor. The simulation results show that the modified model significantly improved the uniformity of the temperature field and the synchronization of the solidification process, with more accurate shrinkage defect predictions. The maximum reduction in shrinkage volume at monitoring points reached 44.2%, and the uniformity of defect distribution was greatly enhanced. Finally, actual pouring of the liner product confirmed that the modified computational model was more consistent with the actual casting in terms of macroscopic forming, hole position accuracy, and defect distribution trends. This study provides a new approach for process simulation optimization of complex porous structure castings and offers practical experience for casting simulation and actual forming of porous products.

Keywords: $ZGMn_{13}Cr_2$, Porous media, Equivalent thermal conductivity model, Investment casting, Numerical simulation

1. Introduction

As a key tool in the development of modern casting processes, numerical simulation technology plays an irreplaceable role in optimizing process parameters and predicting casting defects due to its low cost and high efficiency [1-2]. In particular, in the manufacturing of critical components in fields such as aerospace and energy, accurate temperature field simulation and defect prediction have become core steps in achieving product quality control [3-4]. Research by Chen et al. has shown that optimizing the indirect squeeze casting process through numerical simulation can effectively identify insufficient feeding caused by improper gating system design, providing direct evidence for process improvement [5]. However, when dealing with porous castings with complex internal cavity structures, the accuracy of traditional numerical simulation methods faces severe challenges. Such issues are especially prominent in the production of typical porous structural castings such as electrolytic aluminum electrolyte autogenous mill liners. ProCAST usually simplifies the internal cavity areas of castings as adiabatic spaces or assigns only the thermal properties of air, a treatment that ignores the complex thermal interactions between solid metal and cavities [6]. For high-manganese steel materials such as $ZGMn_{13}Cr_2$, which have poor thermal conductivity, the densely distributed internal cavities further exacerbate the anisotropy of heat flow, leading to abnormal local heat accumulation and dissipation. Gigacher et al. pointed out that high-manganese steel is highly sensitive to thermal stress during solidification, making accurate prediction of its temperature field distribution particularly important [7]. The latest research by Hussein et al. further demonstrated that even with advanced simulation software to optimize the gating system, it is still difficult to completely eliminate micro-defects caused by thermal field distortion [8].

The development of equivalent thermal conductivity theory for porous media provides a new approach to solving the above problems. This theory establishes a macroscopic heat transport model for solid-gas composite systems, providing a theoretical framework for accurately describing the effective thermal properties of porous materials. Recent work by Lasseux and Valdés-Parada on refining macroscopic transport models for porous media has further consolidated the foundation of this theory in engineering applications [9]. Significant achievements have been made in the field of non-metallic materials, such as Carson et al., who, based on composition and temperature data, successfully achieved accurate prediction of the effective thermal conductivity of food using a multi-step prediction method [10]. Shaga et al. achieved coordinated regulation of the microstructure and thermal conductivity of porous ceramics by introducing cement-based binders [11]. In theoretical modeling, Ding Yang systematically studied the mechanism of porosity's influence on the thermal conductivity of materials by combining stochastic models with finite element analysis [12]. Huang Kun developed an efficient prediction method based on inversion algorithms, providing a new solution for calculating the effective thermal conductivity of complex porous structures [13].

Although porous media theory has made significant progress in other material fields, its application in numerical simulation of metal casting still has obvious shortcomings. In a systematic review of investment casting numerical simulation technology, domestic scholar Xu Qingyan affirmed the important role of this technology in process optimization but did not delve into the key issue of thermal property correction for porous structural castings. Existing research mostly focuses on the optimization of traditional process parameters, such as Hu Jiaze, who significantly improved the quality of valve shell castings by improving the gating system and setting chill elements [14]. Wang Yongbo, who successfully solved casting defect problems in aluminum alloy housings by optimizing process parameters [15]. Also, Wei Jianhui et al. and Zhang Yanchao et al., for liner castings of different materials, achieved process optimization and defect control through numerical simulation technology [16-19]. Although these studies demonstrate the wide application of numerical simulation in the casting field, their research perspectives have not touched on the essential impact of internal cavity structures in castings on the thermal behavior during the solidification process.

Based on the above research, this study takes the $ZGMn_{13}Cr_2$ steel porous liner as the research object and innovatively proposes introducing the Bruggeman porous medium equivalent thermal conductivity model into the casting simulation process. The study first calculates the overall porosity based on the actual geometric features of the casting and derives the equivalent thermal conductivity scaling factor using the Bruggeman model. Subsequently, this correction factor is embedded into the ProCAST material database to achieve precise thermal property settings for porous regions. Finally, through systematic experimental verification, the consistency between the simulation results before and after correction and the measured data is compared and analyzed in terms of temperature field distribution, solidification behavior and defect prediction, thereby verifying the effectiveness and engineering application value of this correction method in improving the simulation accuracy of castings with porous structures.

2. Process Parameters and Pouring System Design

2.1. Structural Features of the Part

The research object of this study is the porous liner for an electrolytic aluminum electrolyte self-grinding machine, made of $ZGMn_{13}Cr_2$. $ZGMn_{13}Cr_2$ is a high-manganese steel, belonging to the category of iron-based wear-resistant steels, which exhibits excellent performance under specific conditions. The part drawing is shown in Fig. 1, where Fig. 1(a) is the front view, (b) is the left-side view, and (c) is the cross-sectional view of a screen hole. Measurements indicate that the casting has a thickness of 30 mm and a width of 402 mm. Its interior is densely distributed with 145 conical through-holes, with a single hole volume of 13.3 cm^3. The geometric accuracy requirements for the holes are strict: the front diameter is 18 mm, and the back diameter is 27 mm.

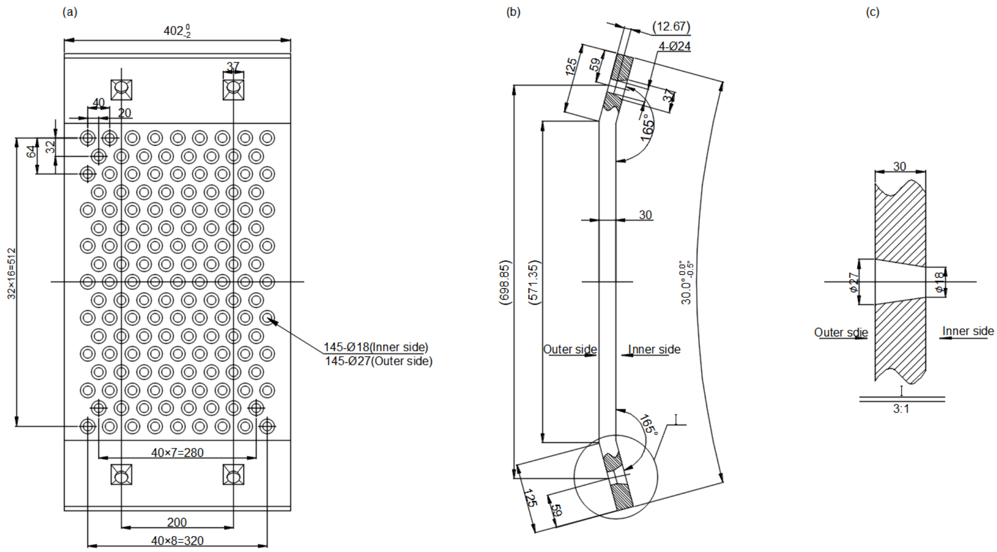

Fig. 1. Schematic diagram of the porous liner structure: (a) Front view, (b) Left view, (c) Sectional view of the sieve hole

2.2. Selection of Casting Process

Given the structural feature of the porous liner containing 145 high-precision tapered through-holes, traditional casting methods find it difficult to accurately reproduce its shape. Due to its outstanding ability to replicate complex structures, high dimensional accuracy, and excellent surface quality, the investment casting process has become the ideal forming solution for this casting. Therefore, this study adopts the investment (lost foam) casting process for the preparation and simulation research of the porous liner.

2.3. Design of the Pouring System

In this study, the formula (6) is used for the design of the gating system. The calculation principle and specific computation method of the Ozhan formula are as follows:

$$F_s=\frac{m}{\rho T\mu\sqrt{2gH_a}} \quad (1)$$

$$H_a=H_0-\frac{P^2}{2C} \quad (2)$$

F_s is the minimum cross-sectional area of the gating system (m²); m is the total mass of metal flowing through the throttling cross-section, approximately equal to the blank mass (kg); g is the value of gravitational acceleration (m/s²);ρ is the density of the molten metal (kg/m³); T is the time to fill the mold cavity (s); μ is the molten metal flow coefficient; H_a is the actual average calculated head during mold filling (m). H_0 is the static head of the molten metal above the throttling section (cm); P is the height of the mold cavity above the throttling section (cm); C is the total height of the casting (mold cavity) (cm).

Through measurement, the volume of a single casting is 8078 cm³, the total pore volume is 1827 cm³, and the casting mass is 77 kg. According to actual process requirements, the final pouring time is determined to be 14 seconds, with a flow coefficient μ = 0.3. The final gating ratio is determined as $S_{vertical}$: $S_{horizontal}$: S_{inner}=1.2:1.1:1, with H_a = H_0. Substituting the measured data into the formula yields F_s = 97 mm². Therefore, $S_{vertical}$: $S_{horizontal}$: S_{inner} = 117 mm² : 107 mm² : 97 mm².
Based on the above information, the specific values of the relevant parameters are shown in Table 1.

Table 1.
Key Geometric Parameters of the Pouring System

Component	Section	Dimensions (mm)
Sprue	Square	40×40×800
Cross runner	Rectangle	60×30×500
Inner runner	Rectangle	30×9×30
Pouring cup	Conical+straight cylinder	Inletφ100→Outlet40×40

In the investment casting process, the design of the gating system directly determines the kinetic behavior and thermodynamic state of molten metal filling the mold cavity, and is a key factor affecting the forming quality of the casting. Considering the characteristics of high-manganese steel $ZGMn_{13}Cr_2$, which is prone to oxidation and has a high thermal shrinkage rate, as well as the complex structure and dispersed hot spots of the porous liner, the selection of the pouring method must prioritize filling stability, control of oxidation and slag inclusion, and the effectiveness of feeding during solidification. Based on preliminary simulation analysis and a comprehensive consideration of the casting's geometry and production stability, this study adopts a middle-pour gating system as the process scheme for subsequent porous media model modification and verification. Theoretically, the middle-pour scheme is more conducive to forming a relatively symmetrical and uniform initial temperature distribution inside the porous liner, which is crucial for effectively verifying and highlighting the correction effect of the porous media model on thermal field simulation.

Based on the above calculations and the key geometric parameters determined in Table 1, a three-dimensional assembly model of the middle-pour gating system and the casting was constructed, as shown in Fig.2. This model intuitively presents the spatial layout relationship between the sprue, runner, ingate, and the porous liner casting, providing an accurate geometric foundation for subsequent simulation analysis.

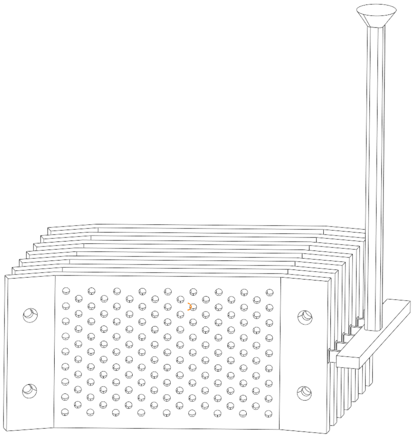

Fig. 2. Three-dimensional assembly model of the middle-pour gating system and casting

3. Modification of the Porous Media Model and Simulation Implementation

In the production process of investment casting for porous liners, the complexity of the pore structure significantly increases the difficulty of designing the gating process. This is because defects such as shrinkage cavities, shrinkage porosity, and gas porosity are prone to occur in areas near the pores, with the core reason being that the pore structure itself disrupts the balance of the casting process. Although the traditional ProCAST simulation method can predict macroscopic flow behavior, it has certain limitations. The conventional Navier–Stokes model treats the pore region as a free-flow space, ignoring the obstructive effects of the porous medium on heat conduction and molten metal flow, which leads to distortion in the simulated flow velocity and temperature field at the pore edges. To address these issues, this study introduces the Bruggeman equivalent thermal conductivity model for porous media, establishing a quantitative relationship between porosity and equivalent thermal conductivity to accurately characterize the mechanism by which the pore structure affects heat conduction.

3.1. Equation for Equivalent Thermal Conductivity

To address the effect of high volume fraction porosity on heat conduction, this study adopts the Bruggeman effective medium model based on mean field theory. This model fully considers the interactions between fillers and is suitable for the high porosity conditions in this study. Its general form is shown in Equation (3):

$$(1-f)^3 = \left(\frac{K_m}{K_e}\right)^{\frac{1+2\alpha}{1-\alpha}} \left[\frac{K_e - K_d(1-\alpha)}{K_m - K_d(1-\alpha)}\right]^{\frac{3}{1-\alpha}} \quad (3)$$

Where, K_e is the effective thermal conductivity; K_m is the thermal conductivity of the metal matrix; K_d is the thermal conductivity of the filler (air); f is the volume fraction of the filler; and α is a dimensionless parameter related to the interfacial thermal resistance.

Given that the pores involved in this study are on the millimeter scale, their specific surface area is much smaller than that of nanocomposites, and the interfacial thermal resistance effect can be neglected. Therefore, letting $\alpha \to 0$, Equation (3) can be simplified to Equation (4):

$$(1-f)^3 = \frac{K_m}{K_e}\left[\frac{K_e - K_d}{K_m - K_d}\right]^3 \quad (4)$$

In the high-temperature environment of the metal casting solidification process, the cavities inside the casting were filled with still air. At around 1500 °C, during solidification, the melt cooled rapidly and the pores became enclosed by the solid metal phase. This significantly shortened the duration of radiative heat transfer and also restricted its heat transfer paths. Furthermore, within millimeter-scale pores, convection was negligible, and heat conduction dominated the heat transfer process. Since the thermal conductivity of high-manganese steel was much higher than that of air, the air phase constituted the dominant thermal resistance in the solid-gas heat transfer path, and its exact thermal conductivity value had no substantial effect on the overall effective thermal conductivity. Introducing a radiation term would have required additional parameters that were difficult to determine accurately—such as emissivity, pore morphology, and view factors—which would only have increased model complexity without yielding corresponding practical benefits. Neglecting radiative heat transfer also helped maintain the model's simplicity and engineering utility. Therefore, in the derivation of this study, the conductive contribution of still air was reasonably neglected by setting Kd $\to 0$, we can obtain:

$$(1-f)^3 = \frac{K_m}{K_e}\left(\frac{K_e}{K_m}\right)^3 = \left(\frac{K_e}{K_m}\right)^2 \quad (5)$$

From this, the expression for the thermal conductivity of the porous medium can be derived as Equation (6):

$$K_e = K_m(1-f)^{3/2} \quad (6)$$

In the specific application scenario of this study, the cavities inside the casting are the fillers dispersed in the metal matrix.

Therefore, the filler volume fraction f is numerically equivalent to the porosity ϕ of the casting, from which expression (7) can be obtained:

$$\phi = f = \frac{V_{pore}}{V_{total}} \quad (7)$$

3.2. Calculation of Relevant Parameters

To achieve physically accurate settings for the thermal property parameters of the porous region, this section based on the actual geometry and material characteristics of the casting, adopts the Bruggeman effective medium theory to systematically calculate the overall porosity and thermal conductivity scaling factor of the casting. The purpose of this calculation is to transform macroscopic geometric features into physical parameters that can be used for simulation correction, thereby enhancing the realism of temperature field and solidification process simulations.

3.2.1. Porosity Calculation

Porosity is a key parameter that characterizes the proportion of pore volume in a porous medium and its value directly affects the accuracy of calculating the effective thermal conductivity. The liner casting studied in this study contains 145 densely distributed conical through-holes, forming a typical porous structure. To accurately assess the impact of the holes on the overall thermal properties, it is first necessary to determine the total porosity of the casting. According to previous geometric measurement data, the solid volume of a single casting is V_{total} = 8078 cm³,and the total volume of all holes is V_{pore} = 1827 cm³.Porosity ϕ is defined as the ratio of the pore volume to the total volume of the casting. Substituting the data into expression (7) yields:

$$\phi = \frac{V_{pore}}{V_{total}} = \frac{1827}{8078} \approx 0.23$$

The calculation results show that the porosity of this porous liner is 0.23, meaning that the hole structure accounts for approximately 23% of the total volume of the casting. This value provides an important input parameter for the subsequent calculation of the effective thermal conductivity scaling factor based on the Bruggeman model.

3.2.2. Scaling Factor

Based on the obtained casting porosity, it is necessary to further calculate the scaling factor of the thermal conductivity to correct the thermal physical parameters of the porous region. In this study, the Bruggeman model, suitable for high-porosity composite systems, is adopted. This model takes into account the interaction between fillers (in this case, air pores), and its simplified form is shown in Equation (8):

$$K_e = K_m(1-\phi)^{3/2} \quad (8)$$

The scaling factor is defined as the ratio of the equivalent thermal conductivity to the matrix thermal conductivity, i.e.,Ke/Km. Substituting the calculated porosity ϕ = 0.23 into the formula, the scaling factor is obtained as:

$$\frac{K_e}{K_m} = (1-0.23)^{3/2} = (0.77)^{1.5} \approx 0.675$$

The calculated scaling factor is approximately 0.675, indicating that due to the presence of pore structures, the effective thermal conductivity of the porous region in the casting decreases to 67.5% of that of the solid material. This factor will be used as a key parameter input into the ProCAST material database to accurately correct the thermal conduction properties of the porous region in the simulation, thereby enhancing the realism of the temperature field and solidification process simulation.

4. Simulation of the Casting Process and Result Analysis Based on the Modified Porous Media Model Theory

To implement the porous media equivalent thermal conductivity model in ProCAST, the calculated scaling factor of 0.675 was uniformly applied to the thermal conductivity of the entire computational domain. This includes both the porous liner body and the gating system. A unified material property was adopted to simplify the simulation setup and maintain consistency in the numerical model.

The gating system primarily serves as a thermal boundary condition for the liner. Its global thermal property adjustment does not compromise the focused investigation on the porous structure. This approach ensures a consistent modeling framework while enabling a targeted evaluation of the model's accuracy in the primary region of interest.

To ensure that the simulation accuracy is not affected by the mesh size, a mesh independence study was conducted in this work. Considering the geometric characteristics of the porous structure in the casting, three global mesh sizes were established: coarse (15 mm), medium (10 mm), and fine (5 mm). The results show that the 15 mm mesh fails to accurately capture fine features such as pores and exhibits poor convergence during solution. Although the 5 mm mesh provides higher accuracy, it leads to excessively high computational cost and cumbersome post-processing. In comparison, the 10 mm mesh ensures satisfactory accuracy in predicting the temperature field, solidification process, and defects in the porous regions while significantly improving computational efficiency. Therefore, all subsequent simulations were performed using this validated 10 mm mesh.

4.1. Selection of Reference Points for Evaluating the Effect of Model Modification

To systematically evaluate the impact of the porous media model modification on the thermal behavior of the casting and the accuracy of defect prediction, representative monitoring points must be set in key areas of the casting. By comparing and analyzing the temperature evolution, solidification process, and defect formation trends at these points before and after modification, the quantitative improvement in simulation fidelity brought by model optimization can be revealed, providing a basis for the scientific adjustment of process parameters.

Based on the geometric structure and pouring characteristics of the porous liner, five representative tracking points were selected for analysis, with their spatial distribution shown in Fig.3 Among them.

Point1 is located in the cavity area far from the pouring gate. The arrival time of molten metal at this point is relatively late, with significant heat loss. It usually solidifies earlier and serves as a typical location for evaluating feeding difficulty and predicting shrinkage defects in remote areas.

Point2 is located in the cavity area near the pouring gate. As a direct heat source influence zone, its solidification behavior reflects the impact of continuous feeding by high-temperature molten metal on the thermal state of the cavity.

Point3 is located in the cavity at the center of the casting. As a typical hot spot area, its solidification process can be used to determine the overall solidification sequence and the core's structural density.

Point4 and Point5 are located in the upper and lower boundary pore regions of the casting, respectively. Together, they are used to evaluate the influence of the mold shell boundary cooling effect on the solidification behavior of the pores, particularly the solidification asymmetry caused by differences in heat dissipation conditions between the upper and lower parts.

These five monitoring points together form a spatial control network for assessing the thermal response and defect sensitivity of the porous region. The data will provide key support for the quantitative comparison and analysis of the subsequent model correction effects.

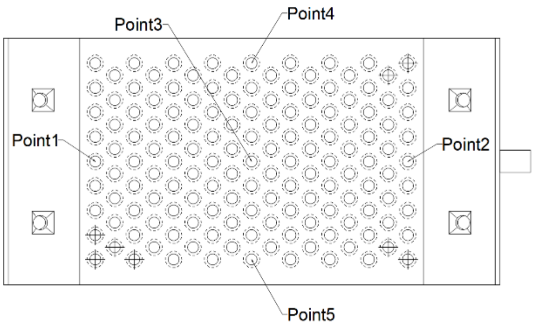

Fig. 3. Layout diagram of positioning points for evaluating model correction effects

4.2. Simulation Results Analysis

4.2.1. Temperature Field Distribution

The uniformity of the temperature field distribution is the key to achieving sequential solidification of the casting and controlling thermal stress and shrinkage defects. To quantitatively evaluate the impact of the model correction on the internal thermal state of the casting, this section compares and analyzes the temperature–time curves at each monitoring point before and after the correction, as shown in Fig.4.

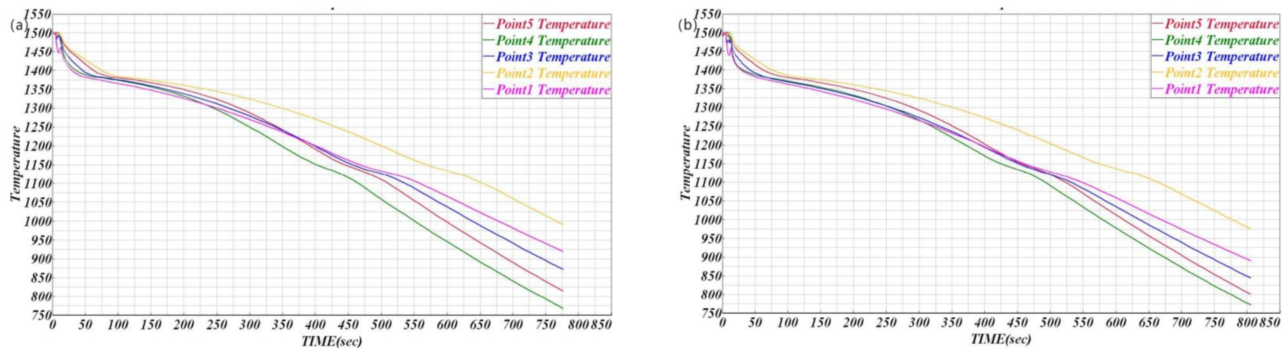

Fig. 4. Comparison of temperature distribution curves at positioning holes before and after model correction: (a) Temperature distribution curve of the central injection positioning hole before correction (b) Temperature distribution curve of the central injection positioning hole after correction

From the comparison of the temperature curves shown in Fig.4(a) and 4(b), it can be seen that the model correction significantly improved the uniformity of the temperature field distribution inside the casting. In the simulation results before correction (Fig 4(a)), the temperature curves of each monitoring point are scattered along the time axis. The curve of Point4 (upper boundary) and Point2 (near the gate) are located at opposite extremes of the temperature range, while the curves of Point1, Point3, and Point5 are distributed at different temperature levels, together forming a divergent temperature distribution pattern.

In contrast, in the system after model modification (Fig.4(b)), the distribution of the temperature field has been optimized. The four temperature curves of Point1, Point3, Point4, and Point5, representing the far end, core, and boundary of the casting, are closely aligned, showing a highly convergent distribution pattern. This intuitive change in the image indicates that the optimized model effectively reduces the temperature differences in most areas of the casting during the solidification process, which directly helps to lower thermal stress caused by uneven cooling and creates ideal thermal field conditions for achieving balanced sequential solidification.

4.2.2. Solidification Process

The synchronization of the solidification process is key to achieving sequential solidification and controlling shrinkage defects. To quantitatively evaluate the impact of model modification on solidification behavior, this section compares and analyzes the solidification curves (solid fraction–time curves) at each monitoring point before and after modification, with the results shown in Fig.5.

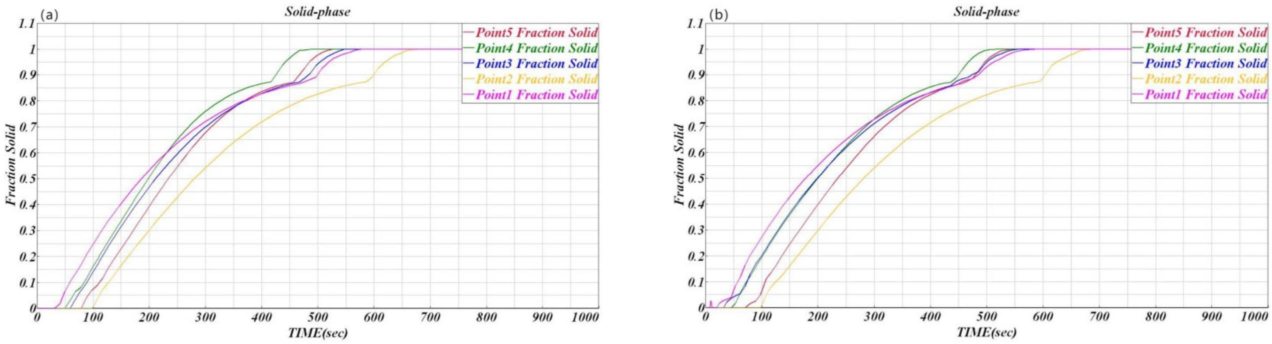

Fig. 5. Solidification curves of positioning holes before and after model modification: (a) Solidification curves of positioning holes with central pouring before modification (b) Solidification curves of positioning holes with central pouring after modification

By comparing Fig.5(a) and (b), it can be intuitively observed that the model modification significantly optimized the solidification coordination among different regions inside the casting. In the pre-modification simulation (Fig.5(a)), the solidification paths of each monitoring point were scattered along the time axis, showing a pronounced asynchrony in the solidification sequence. Specifically, Point1, located far from the gate, experienced the fastest heat loss and thus began and completed solidification first, while Point2, directly influenced by the heat source, suffered a severe delay in its solidification process due to continuous reception of high-temperature molten metal. This large solidification time difference directly led to asynchronous feeding demands in different regions. When remote areas such as Point1 had already solidified and closed, losing their feeding capability, regions near the gate such as Point2 were still in a liquid or mushy state and required feeding, thereby greatly increasing the risk of shrinkage defects in the latter.

In contrast, in the system modified with the porous media model (Fig.5(b)), the solidification behavior at each monitoring point was significantly improved, exhibiting highly coordinated solidification paths. The solidification curves representing the casting's remote end (Point1), central hot spot (Point3), and bottom (Point5) were closely aligned, with markedly enhanced convergence. This change indicates that the optimized model effectively reduced the solidification time differences between key feature regions of the casting. The improved synchrony in the solidification process means that the feeding windows of various regions overlap more in time, which is conducive to establishing longer-lasting and more effective feeding channels.

4.2.3. Cooling Behavior Evolution

The uniformity of cooling rate distribution is a key factor affecting the solidification microstructure, residual stress, and defect formation in castings. To quantitatively evaluate the impact of model modification on heat exchange behavior, this section compares and analyzes the cooling rate curves at each monitoring point before and after modification, with the results shown in Fig.6.

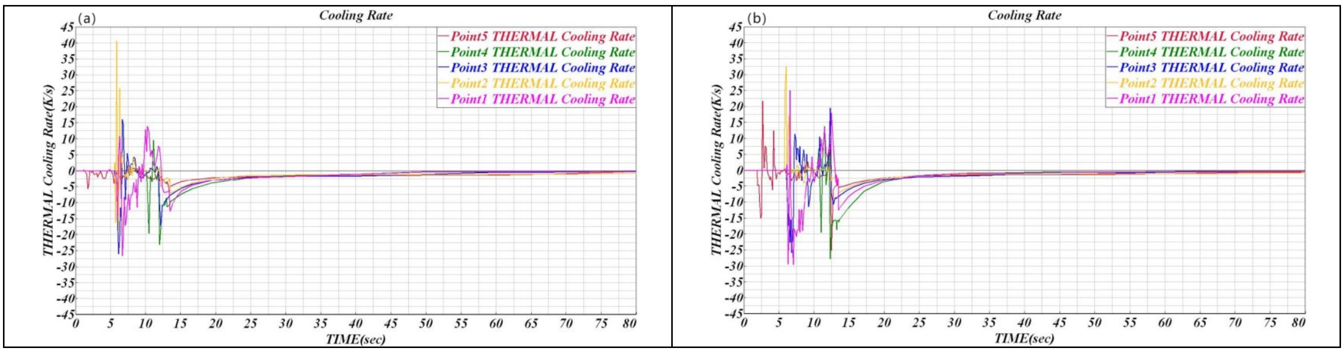

Fig. 6. Comparison of cooling rate curves at positioning holes before and after model correction: (a) Cooling rate curve of the central injection positioning hole before correction (b) Cooling rate curve of the central injection positioning hole after correction

In the system before model correction (Fig.6(a)), the cooling rate curves at each monitoring point exhibit significant local differences and non-uniformity. Quantitative analysis of the curve characteristics shows that at Point2, the fluctuation between peak and trough around 5.5 seconds reaches as high as 57°C; while at Point4, the cooling rate remains at a relatively low level after 10.5 seconds, lacking a distinct active cooling phase. This pronounced temperature fluctuation combined with sluggish boundary heat dissipation behavior indicates that the traditional model, by neglecting the obstruction of heat flow caused by the porous structure, severely distorts the simulation of local heat exchange.

In contrast, the system corrected with the porous media model (Fig.6(b)) demonstrates a more balanced and reasonable thermal evolution. The curve comparison clearly shows that the fluctuation range at Point2 decreases from 57°C to 32°C, a reduction of about 44%, and transforms into a smoother single cooling trend; meanwhile, Point4 exhibits a significant cooling phase at the corresponding time, consistent with physical expectations. These systematic changes consistently indicate that the optimized model, by introducing a more realistic equivalent thermal conductivity, effectively corrects the abnormal local heat accumulation and transfer caused by distorted thermal property parameters, making the overall simulated heat exchange process more uniform.

4.2.4. Casting Defect Analysis

Shrinkage cavities and porosity are typical defects formed during the casting process due to ineffective feeding during liquid and solidification shrinkage, and their distribution characteristics directly affect the density of porous castings. This section compares and analyzes the porosity evolution curves and the three-dimensional morphology of shrinkage cavities at each monitoring point before and after model correction, with the results shown in Fig.7 and 8.

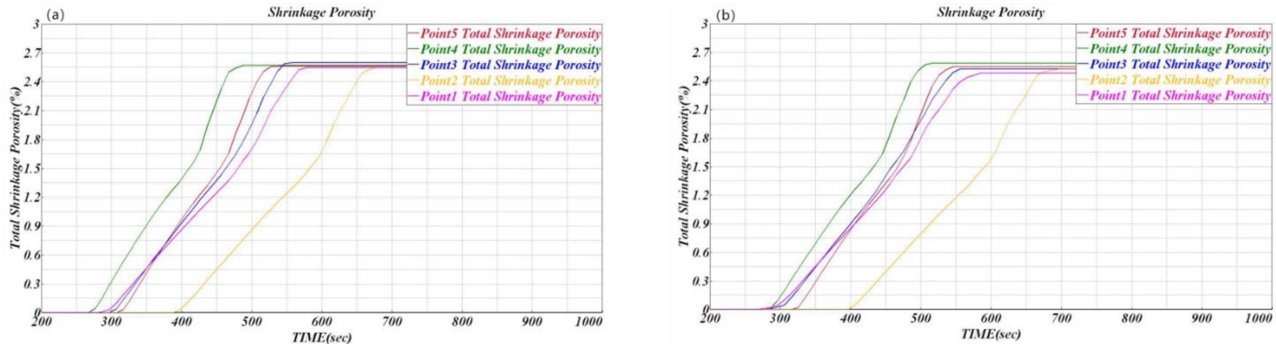

Fig. 7. Shrinkage–time curves of positioning holes before and after model correction: (a) Shrinkage–time curve of positioning holes before correction in the central pouring method (b) Shrinkage–time curve of positioning holes after correction in the central pouring method

Analysis of the porosity evolution curves shows that the model correction optimized the uniformity of defect distribution. Observing the pre-correction curves (Fig.7(a)), the defect formation behavior at each monitoring point is temporally dispersed, with differences in the final porosity levels. Point1's porosity begins to rise sharply at about 280 seconds, while Point2, Point3, Point4, and Point5 start to increase significantly at around 397 seconds, 300 seconds, 265 seconds, and 310 seconds respectively, with final values ranging from 2.55 to 2.60. In contrast, the corrected system (Fig.7(b)) exhibits higher coordination, with the time points at which porosity begins to rise significantly being more concentrated, and the final peak porosity values generally reduced—Point1 decreases from 2.55 to 2.48, Point3 from 2.60 to 2.53, and the differences between the stable values of all monitoring points are significantly narrowed.

To evaluate the impact of model correction on defect morphology and distribution at multiple scales, this study combines overall and local views for comparative analysis. Figures 8a and 8b respectively show the overall shrinkage cavity distribution of the casting before and after correction. To more clearly observe the details of defect morphology, a corresponding local magnification of the central area (monitoring point Point3) is further provided. A direct comparison of the overall images reveals obvious differences in shrinkage cavity distribution after correction compared to before. The local magnification more clearly shows that the shrinkage cavity morphology in the central area changes after correction, with a visually significant feature being the reduction in individual size. To quantitatively reveal the specific extent of this difference, the shrinkage cavity volumes at each monitoring point were precisely measured, with the results shown in Table 2.

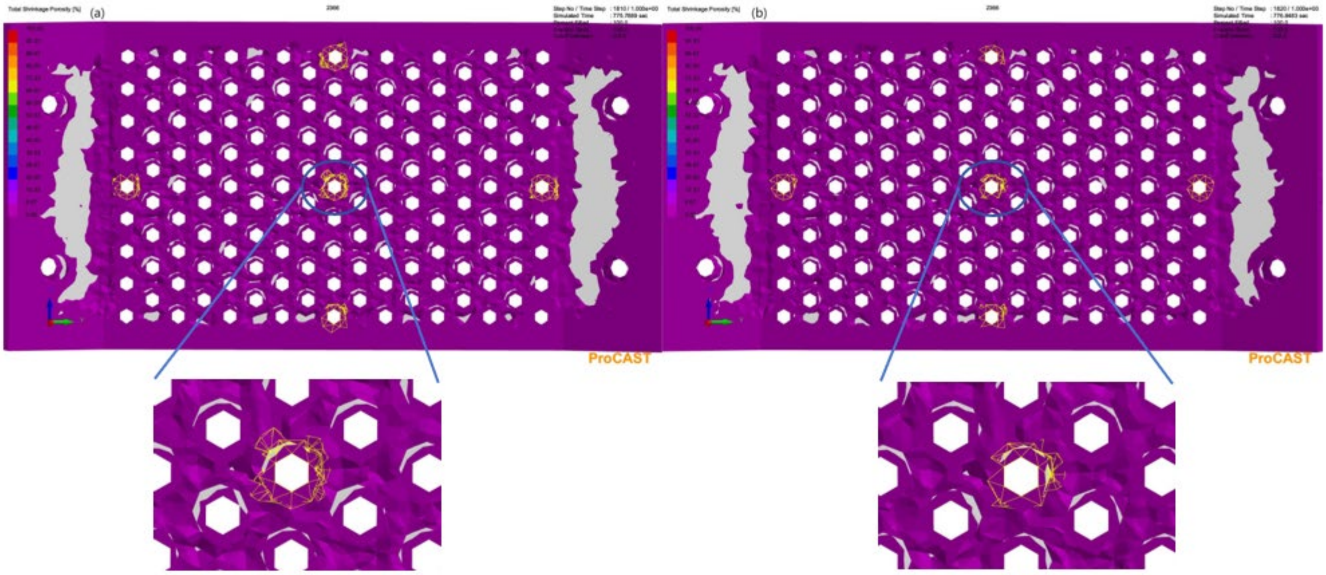

Fig. 8. Distribution of shrinkage porosity at positioning points before and after model correction: (a) Distribution before correction (b) Distribution after correction

Table 2.
Comparison of defect simulation results before and after correction

Monitoring Point Location	Shrinkage Cavity Volume Before Modification (cm³)	Shrinkage Cavity Volume After Modification (cm³)	Volume Reduction
Center Hole	0.240	0.157	34.6%
Upper Boundary Hole	0.165	0.092	44.2%
Left Boundary Hole	0.148	0.107	27.7%
Right Boundary Hole	0.122	0.092	24.6%
Lower Boundary Hole	0.121	0.108	10.7%

The quantitative data in Table 2 provides strong support for the morphological changes shown in Figure 8 and reveals the following two key optimization trends:

1) Significant reduction in total defect volume: After model correction, the shrinkage cavity volume at all five monitoring points decreased markedly. In the central hole area, where the hot spot effect is most pronounced, the shrinkage cavity volume dropped from 0.240 cm³ to 0.157 cm³, a reduction of 34.6%; the shrinkage cavity volume at the upper boundary hole decreased even more significantly, by 44.2%. This data demonstrates that the corrected model, by more realistically characterizing the thermal properties of porous regions, effectively improves the overall feeding efficiency of the casting.
2) Substantial improvement in defect distribution uniformity: Before correction, the shrinkage cavity volumes at different monitoring points varied greatly, with a maximum difference of 0.118 cm³, reflecting the lack of coordination in the feeding process and severe unevenness in defect distribution predicted by the traditional model. After correction, the differences in shrinkage cavity volumes among the points were greatly reduced, with the maximum difference significantly decreasing to 0.065 cm³. This key data indicates that the model correction effectively enhances the solidification coordination across different regions of the casting, fundamentally transforming defect distribution from "localized concentration" to "overall uniformity."
3) Analysis of differential shrinkage reduction at boundary holes: The large disparity in shrinkage reduction between the upper (44.2%) and lower (10.7%) boundary holes is explained by solidification fundamentals and validated by the model:
   Thermal Gradient: The upper hole cools faster, solidifies earlier, and forms a feeding choke. The lower hole, near the hotter gating system, solidifies later with a longer feeding path.
   Metallostatic Pressure: Higher pressure at the lower hole inherently suppresses shrinkage, so the unmodified baseline already performs better there, leaving less room for relative improvement.
   Model Effect: The correction amplifies these physical trends: it accentuates the top's feeding difficulty (larger correction) and better simulates the bottom's favorable conditions.

This confirms the model accurately resolves the spatial heterogeneity in solidification caused by thermal and pressure gradients.

The analysis in this section proves that the model correction significantly improves the accuracy of defect prediction. The morphological comparison in Figure 8 and the quantitative data in Table 2 together show that, with the introduction of the porous medium equivalent thermal conductivity model correction, the simulation system can more precisely replicate the thermal behavior and feeding mechanism of hole regions during solidification. This optimization not only achieves a significant reduction in total defect volume but also brings about a substantial improvement in defect distribution uniformity. This dual enhancement in quantitative indicators greatly strengthens the reliability of simulation predictions regarding the internal quality of porous structure castings, particularly in defect control capability.

5. Model Verification and Casting Quality Analysis

To verify the reliability of the simulation scheme modified based on the porous media model, this section conducts experimental validation of the optimized middle-pour casting scheme through actual investment casting tests. By systematically analyzing the macro morphology, dimensional accuracy, and defect distribution of the castings, and comparing them with the modified simulation results, a closed-loop verification from numerical simulation to physical experiment is achieved.

5.1. Process Experiment and Quality Verification

This practical pouring experiment strictly followed the lost foam casting process, with the key steps as follows:

1) Model preparation and cluster assembly: Foam plastic was used to make the liner model, which was then assembled with the gating system (consisting of a sprue and runners) into a complete mold cluster. No separate risers were used, as the casting's relatively uniform wall thickness and the designed gating system were intended to provide adequate feeding**.** The surface of the mold cluster was coated with refractory coating, and after multiple cycles of dipping, sand sprinkling, and drying, a coating with certain strength and permeability was formed.
2) Sand filling and vibration compaction: The coated mold cluster was placed into the sand box, dry sand was gradually filled in, and mechanical vibration was applied to ensure the sand fully filled the internal cavities and surrounding gaps of the model, guaranteeing the compactness of the molding sand and the stability of the mold.
3) Pouring and model gasification: $ZGMn_{13}Cr_2$ high manganese steel was melted using a medium-frequency induction furnace. Once the molten metal reached a temperature of 1500±10°C and deoxidation was completed, pouring was carried out. During pouring, the high-temperature molten metal rapidly vaporized and decomposed the foam mold, and the molten metal gradually filled the cavity previously occupied by the model. The pouring process was kept smooth and continuous, with a total pouring time controlled at about 14 seconds, consistent with the preset simulation parameters.
4) Cooling and sand removal: After pouring is completed, the casting is naturally cooled in the sand mold to reduce thermal stress. Once the casting has completely cooled to room temperature, vibration is used to remove the sand and separate the casting from the mold sand, and a grinding wheel cutting machine is used to remove the gating and riser system.
5) Key points in process control: During pouring, the pouring speed must be kept uniform to avoid interruptions or turbulence, ensuring smooth mold filling. Attention should also be paid to the smooth discharge of vaporized products from the mold cluster to prevent casting defects caused by poor vaporization.

5.2. Casting Results and Model Verification Analysis

To verify the accuracy of the simulation results corrected by the porous media equivalent thermal conductivity model, this section systematically compares the macroscopic quality of the actual castings with the key results predicted by the simulation. The results show that the optimized simulation exhibits good consistency with the actual castings in multiple key quality indicators.

1. **Verification of hole position forming accuracy and dimensional consistency**

The macroscopic appearance of the actual castings is shown in Fig.9(a). It can be seen that all 145 internal conical through-holes are completely and clearly reproduced, with uniform distribution of hole positions, regular geometric shapes, dimensional accuracy meeting design requirements, and clear casting contours without deformation.

This high-precision structural reproduction capability is directly related to the more uniform temperature field distribution predicted by the corrected simulation. A uniform thermal field is a prerequisite for ensuring balanced solidification of the molten metal, thereby obtaining castings with high dimensional accuracy. The excellent hole position accuracy of the actual casting verifies the correctness of the corrected model in predicting the macroscopic temperature field and solidification behavior.

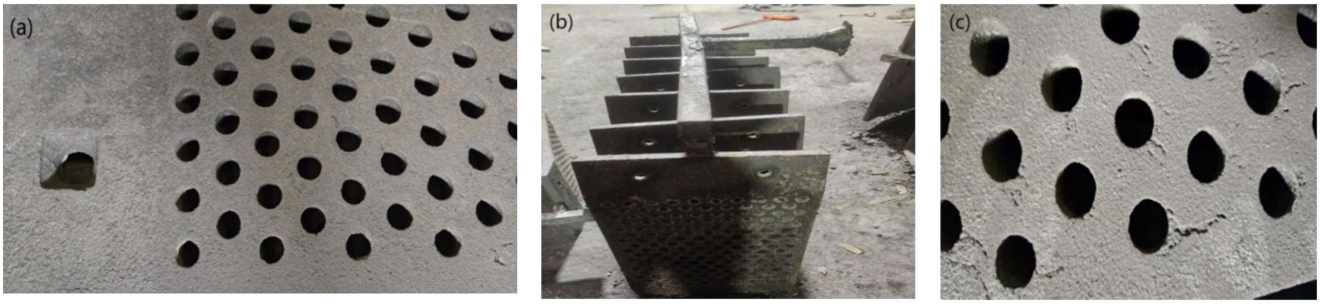

Fig. 9. Macroscopic morphology of the actual poured casting: (a) Image of a single liner surface (b) Image of the overall pouring (c) Image of surface defects

2. Verification of mold filling integrity and flow stability

Fig.9(b) shows the overall casting including the pouring system. The casting profile is full, with solid connections between all parts, and no underfilling or obvious cold shuts or other mold filling defects, indicating that the molten metal filled the entire cavity smoothly and completely.

Simulation Comparison and Conclusion: The filling effect matches the steady filling process obtained in the simulation based on the central pouring scheme and the modified model. The optimized simulation shows that the molten metal can smoothly fill the complex cavity, which is corroborated by the complete forming quality exhibited by the actual casting.

3. Verification of defect distribution trend and prediction accuracy

Macroscopic observation of the working surface of the casting (Fig.9(c)) shows that the surface of the holes only exhibits normal roughness caused by sand cleaning, with no concentrated distribution of macroscopic shrinkage cavities or cracks. This key quality feature is consistent with the fine and dispersed defect distribution trend predicted by the modified model, and stands in sharp contrast to the concentrated defect distribution predicted by the unmodified model, strongly demonstrating the effectiveness of the model modification in improving defect prediction accuracy.

Systematic comparison reveals that the uniform temperature field, steady filling process, and dispersed defect distribution trend predicted by the simulation scheme based on the modified model are successfully reflected in the high hole position accuracy, complete macroscopic morphology, and absence of macroscopic shrinkage cavities in the actual castings. This multidimensional consistency fully proves that introducing the Bruggeman porous media equivalent thermal conductivity model into casting simulation is correct and of practical value for improving the reliability of process optimization for complex porous structure castings.

6. Conclusion

This research study investment casting $ZGMn_{13}Cr_2$ porous liner under different thermal conductivity model. To solve the problem of distortion in traditional numerical simulations caused by dense internal pores during the investment casting process, the Bruggeman porous medium equivalent thermal conductivity model was innovatively introduced and its correction effect verified. By comparing and analyzing the simulated predictions of the temperature field, solidification process, cooling behavior, and shrinkage defects of castings under different thermal conductivity models, the results were finally validated through the macroscopic morphology, dimensional accuracy and defect distribution of the actual castings. The main conclusions of the study are as follows:

1) A physical model-based correction of thermal property parameters was constructed and implemented. The Bruggeman porous medium equivalent thermal conductivity model was successfully introduced into casting simulation, and based on the solid volume and pore volume of the casting, an overall porosity of 23% was accurately calculated. From this, an equivalent thermal conductivity scaling factor of 0.675 was derived. By embedding this correction factor into the ProCAST material database, a physically accurate setting of thermal property parameters for porous regions was achieved.
2) The model correction significantly improved the accuracy of simulation predictions. The corrected simulation showed superior performance in temperature field uniformity, solidification process synchronization, and balanced cooling behavior. Simulation results indicated that after correction, the shrinkage cavity volume at each monitoring point was generally and significantly reduced (with a maximum reduction of 44.2%), and the uniformity of defect distribution was substantially improved. The maximum volume difference between points decreased from 0.118 cm^3 to 0.065 cm^3, demonstrating higher reliability in predicting shrinkage defects with the modified model.
3) Actual casting trials verified the effectiveness of the optimized scheme. The castings produced according to the corrected simulation plan exhibited complete macroscopic morphology, pore position accuracy meeting design requirements, and no severe defects such as macroscopic shrinkage cavities on critical working surfaces. The high internal quality and uniform defect distribution characteristics of the actual castings closely matched the prediction trends of the corrected model. The study confirmed at the physical experiment level that this model correction method is effective and of practical engineering value in guiding the process design of complex porous structure castings.

Acknowledgments

This research was financially supported by the Guizhou Industry Simulation Design & Innovation Center (Grant No. QKZYD [2016]4006). Additional, she is also supported by the Guizhou Provincial Laboratory Research Project (Grant Nos. QK Platform ZSSYS[2025]ZD007) and the Guizhou Provincial Department of Education's "Hundred Schools and Thousand Enterprises Technology Research and Development" Project, China (Grant No. [2024]003).

References

[1] Zhengyang, C., Yueyang, L., Fengrui, Z., Shi, L. & Ji, Z. (2022). Progress in numerical simulation of casting process. *Measurement and Control*. 55(5-6), 257-264. https://doi.org/10.1177/00202940221102656.

[2] Xu, Q.Y. (2022). Research progress in numerical simulation of investment casting process. *Foundry (China)*. 71(07), 803-813. https://kns.cnki.net/kcms2/article/abstract?v=SHX-2ztJhdcCo3uZgMOckLCRj_9tp6Nra_1qERjCogS8Mubv23LaCBXIE3FDXJRddsH5ykiGIij-dHze8BquEYrhIGXFvVgzO1W7f0PFp5LogXcaN3BCsEYusnPz2wnoDgGSPMloM-SGjDkX83dwS-t_GJjX9WBzPfJFgUippKXezMt39GwXqZd5QHiXZTEJ&uniplatform=NZKPT&language=CHS.

[3] Yang, X., Zhang, L., Lai, C., Li, S., Li, M. & Deng, Z. (2018). A method to control the transverse corner cracks on a continuous casting slab by combining microstructure analysis with numerical simulation of the slab temperature field. *Steel Research International*. 89(5), 1-8. https://doi.org/10.1002/srin.201700480.

[4] Rathod, H., Dhulia, J.K. & Maniar, N.P. (2017). Prediction of shrinkage porosity defect in sand casting process of LM25. *IOP Conference Series: Materials Science and Engineering*. 225(1), 1-8. DOI: 10.1088/1757-899X/225/1/012237.

[5] Chen, L., Li, J., Zhao, Y., Li, M., Li, L., Chen, L. & Hou, H. (2020). Numerical simulation and optimization of indirect squeeze casting process. *Engineered Science*. 13, 65-70. https://doi.org/10.30919/es8d1157.

[6] Abdullin, A.D. (2017). New capabilities of the ProCAST 2017 software in simulating casting processes. *Metallurgist*. 61(5-6), 433-438. https://doi.org/10.1007/s11015-017-0513-x.

[7] Gigacher, G., Pierer, R., Wiener, J. & Bernhard, C. (2006). Metallurgical aspects of casting high-manganese steel grades. *Advanced Engineering Materials*. 8(11), 1096-1100. https://doi.org/10.1002/adem.200600152.

[8] Hussein, A., Ahmed, M.R., Abid, H., Meshal, A., Ben, F.L. & Anjum, B.I. (2022). Effects of gating design on structural and mechanical properties of high manganese steel by optimizing casting process parameters. *Journal of Mechanical Science and Technology*. 36(8), 3931-3937. https://doi.org/10.1007/s12206-022-0715-4.

[9] Lasseux, D. & Parada, F.J.V. (2025). Corrigendum to "Simplifications of macroscopic models for heat and mass transfer in porous media". *Advances in Water Resources*. 205, 105073, 1-4. https://doi.org/10.1016/j.Advwatres.2025.105073.

[10] Carson, J.K., Wang, J., North, M.F. & Cleland, D.J. (2016). Effective thermal conductivity prediction of foods using composition and temperature data. *Journal of Food Engineering*. 175, 65-73. https://doi.org/10.1016/j.jfoodeng.2015.12.006.

[11] Shaga, A., Duan, L.L., Chen, X. & Zhang, X.J. (2025). Microstructure-controllable Al2O3 porous ceramics via cementitious agent-modified freeze casting and ambient curing. *Ceramics International*. 51(27A), 53047-53052. https://doi.org/10.1016/j.Ceramint.2025.09.035.

[12] Ding, Y., Deng, M.Y., Zhou, S.X., Wang, Z.P., Dong, J.L. & Wei, Y.Q. (2019). he Evolution Relation Between Materials' Porosity and Thermal Conductivity Based on the Simulation by COMSOL® Software. *Materials Reports*. 33(S1), 211-215.

[13] Huang, K. (2021). *Research on prediction methods for effective thermal conductivity of porous media*. Master's thesis, Dalian University of Technology. https://link.cnki.net/doi/10.26991/d.cnki.gdllu.2021.000867.

[14] Hu, J.Z., Du, H.H., Liu, H.Y., Li, G.Y. & Fan, X.R. (2025). Research on the optimization of sand casting process for valve shell parts based on ProCAST numerical simulation. *Metal Working*, 1-7. https://link.cnki.net/urlid/11.5627.TH.20250917.1739.004.

[15] Wang, Y.B., Meng, Z.Y., Zhang, X.Q., Zhang, R.Q. & Zhu, C.L. (2025). Numerical simulation and process optimization of aluminum alloy shell investment casting. *China Foundry Machinery & Technology*. 60(04), 80-84.

[16] Wei, J.H. & Jiang, M.Q. (2020). Optimization design of investment casting process for K423 liner based on ProCAST. *Special Casting & Nonferrous Alloys*. 40(11), 1259-1261. https://doi.org/10.15980/j.tzzz.2020.11.018.

[17] Zhang, Y. C., Xiao, Z. X., Liang, G. X., Zhang, H. R., Zhang, L., Liu, X. L. & Feng, J. H. (2024). Evaluation of lost foam casting process for high manganese steel liner based on finite element simulation. *Special Casting & Nonferrous Alloys*. 44(11), 1528-1535. https://doi.org/10.15980/j.tzzz.2024.11.013.

[18] ZHY. (2025). *Numerical Simulation Assisted Optimization of Gray Cast Iron Bearing Seat Casting Process.* Retrieved October 15, 2025, from https://www.zhycasting.com/numerical-simulation-assisted-optimization-of-gray-cast-iron-bearing-seat-casting-process/?utm_source=chatgpt.com

[19] Bruggeman, D.A.G. (1935). Calculation of Various Physical Constants of Heterogeneous Substances. I. Dielectric Constants and Conductivities of Composite Bodies Made of Isotropic Substances. *Annalen der Physik.* 416(7), 636-679. https://doi.org/10.1002/andp.19354160705. (in German).